where δH_{TZ}^i, $(V_{\mathrm{S}}^{410})_i$, and $(V_{\mathrm{S}}^{660})_i$ are the data at the i-th station ($i = 1,\ldots,8$) and $\delta H_{\mathrm{TZ}}(\ldots)$ is a function of the variables γ_{410} and γ_{660}. The cumulative errors σ_i are computed for δH_{TZ}^i and account for uncertainties of t_{diff}^i, $(V_{\mathrm{S}}^{410,660})_i$, R, and $\partial \ln V_{\mathrm{S}}/\partial T$. The solution (Fig. 5A) is consistent with the mineralogic Clapeyron slopes of the olivine transformations (14). The width of the error ellipses accounts for our measurement uncertainties as well as for possible lateral variations in R ($\pm 40\%$) and $\delta \ln V_{\mathrm{S}}/\delta T$ ($\pm 30\%$). Unlike the slope of the straight line in Fig. 4B, the solution of Eq. 1 is not sensitive to the two extremal data points; excluding either or both results in a small displacement of the best-fit point and a slight widening of the 1σ ellipses (Fig. 5B).

The correlation between t_{diff} and $V_{\mathrm{S}}^{\mathrm{TZ}}$ (and thus between the TZ thickness and temperature) in East Asia–Australia (Fig. 4) contrasts the weak correlation inferred from global t_{diff} data sets and tomographic models (12, 13, 29). We suggest that this inconsistency is due to differences in spatial resolution of t_{diff} measurements, on the one hand, and of $V_{\mathrm{P}}^{\mathrm{TZ}}$ or $V_{\mathrm{S}}^{\mathrm{TZ}}$ values from global tomography, on the other. The resolution of global wavespeed heterogeneity in the TZ is most uniform (30, 31) at wavelengths that are much larger (>3000 km) than the spatial resolution of the t_{diff} measurements (≈ 500 km), and this may obscure existing $t_{\mathrm{diff}} - V_{\mathrm{S}}^{\mathrm{TZ}}$ correlations. Our study, in which t_{diff} and $V_{\mathrm{S}}^{\mathrm{TZ}}$ relate to the same spatial length scale, corroborates models in which the phase transformations in olivine cause both 410 and 660.

References and Notes

1. J. D. Bernal, *Observatory* **59**, 265 (1936).
2. D. L. Anderson, *Science* **157**, 1165 (1967).
3. A. E. Ringwood, *Earth Planet. Sci. Lett.* **5**, 401 (1969).
4. E. Ito, E. Takahashi, *J. Geophys. Res.* **94**, 10673 (1989).
5. T. Katsura, E. Ito, *J. Geophys. Res.* **94**, 15663 (1989).
6. G. Helffrich, *Rev. Geophys.* **38**, 141 (2000).
7. P. M. Shearer, in *Earth's Deep Interior: Mineral Physics and Tomography from the Atomic to the Global Scale*, S. Karato, A. M. Forte, R. C. Liebermann, G. Masters, L. Stixrude, Eds. (Geophysical Monograph 117, American Geophysical Union, Washington, DC, 2000), pp. 115–131.
8. S.-H. Shim, T. S. Duffy, G. Shen, *Nature* **411**, 571 (2001).
9. L. Chudinovskikh, R. Boehler, *Nature* **411**, 574 (2001).
10. T. Irifune *et al.*, *Science* **279**, 1698 (1998).
11. K. Hirose, Y. Fei, S. Ono, T. Yagi, K. Funakoshi, *Earth Planet. Sci. Lett.* **184**, 567 (2001).
12. S. Chevrot, L. Vinnik, J.-P. Montagner, *J. Geophys. Res.* **104**, 20203 (1999).
13. M. P. Flanagan, P. M. Shearer, *J. Geophys. Res.* **103**, 2673 (1998).
14. C. R. Bina, G. R. Helffrich, *J. Geophys. Res.* **99**, 15853 (1994).
15. Because phase transformations in the Earth occur over depth intervals in which multiple phases coexist, it is not meaningful to define the Clapeyron slopes at 410 or 660 thermodynamically (14). The discontinuities, however, are seen as sharp interfaces by finite-frequency seismic waves, and measurements of the depths to these apparent interfaces can constrain the effective ("seismic") Clapeyron slopes at the discontinuities which, although weakly dependent on seismic-wave frequency, otherwise are determined only by thermodynamic properties

(14). The seismically derived Clapeyron slopes can also be affected by isostructural phases with variable chemistry at the depth of the discontinuities (32), in particular because of the exchange of magnesium and iron between olivine and other mantle minerals (33, 34). According to the phase diagrams from (5), a 1% increase in the magnesium number Mg# = Mg/(Mg+Fe) would raise the pressure of $\alpha \rightarrow \beta$ by 0.1 GPa (increasing the depth to 410 by $\delta d_{410} \approx 3$ km), the same effect as from a 35 K increase in temperature [given $\gamma_{410} = 2.9$ MPa/K (14)]. With P and S velocities ($V_{\mathrm{P,S}}$) also growing with Mg# (33), lateral variations in Mg# would thus weaken the thermally induced anticorrelation between d_{410} and $V_{\mathrm{P,S}}$ depicted in Fig. 1A. Our observation that the "seismic" Clapeyron slopes agree (within uncertainties) with the mineralogical slopes for Mg_2SiO_4 is consistent with the actual effect of composition being small.
16. D. J. Weidner, Y. Wang, in *Earth's Deep Interior: Mineral Physics and Tomography from the Atomic to the Global Scale*, S. Karato, A. M. Forte, R. C. Liebermann, G. Masters, L. Stixrude, Eds. (Geophysical Monograph 117, American Geophysical Union, Washington, DC, 2000), pp. 215–235.
17. A downwarp of 660 and an uplift of 410 have been documented beneath the "cold" subduction zones (35, 36), but these regions represent only a small fraction of the upper mantle, possibly with compositional and kinetic effects affecting the phase transformations (16). At larger scales, there is evidence both for and against a δd_{410}–δd_{660} anticorrelation (6, 7), but this may be inconclusive owing to the possibly incoherent temperature variations in the upper and lower TZ (13) and to uncertainties of the measurements (errors in the models of the heterogeneous mantle above 410 translate into substantial uncertainties in inferred discontinuity depth). The measurements of H_{TZ} are generally more precise than those of $\delta d_{410,660}$, because H_{TZ} can be constrained with observables that to first order do not depend on structure above 410, such as the $t_{\mathrm{diff}} = t_{P660s} - t_{P410s}$ that we use here. However, a recent global compilation of converted-wave differential times $t_{\mathrm{diff}} = t_{P660s} - t_{P410s}$ (which scale with H_{TZ}) showed poor correlation with seismic velocities from global tomographic models (12). A similarly weak correlation was obtained by mapping H_{TZ} with long-period SS precursors (13).
18. S. Lebedev, G. Nolet, in preparation.
19. F. J. Simons, A. Zielhuis, R. D. van der Hilst, *Lithos* **48**, 17 (1999).
20. L. P. Vinnik, *Phys. Earth Planet. Int.* **15**, 39 (1977).
21. B. Efron, R. Tibshirani, *Science* **253**, 390 (1991).
22. For each station, we collected all available traces and inspected them visually, rejecting those with strong

background noise before the P-wave onset. After the rotation and deconvolution, we also discarded traces with the SV-component amplitude exceeding 15% of that of the P wave. Finally, we rejected the data if $P410s$ or $P660s$ arrivals could not be identified on the stacks (presumably due to multipathing caused by strong upper-mantle heterogeneity or small-scale discontinuity undulations). The number of records that contribute to the stacks ranges from 13 to 135, with an average of 53 (37).
23. We stack the records from events at different azimuths and distances so that the piercing points of Pds waves at the discontinuities are distributed over an area a few hundred kilometers wide (Fig. 1B). Taking into account the 100- to 300-km width of the Fresnel zone of the waves at the discontinuities [see (12) for discussion], we estimate the lateral resolution of the measurements at ≈ 500 km.
24. Supplementary Web material is available on *Science* Online at www.sciencemag.org/cgi/content/full/296/5571/1300/DC1.
25. B. L. N. Kennett, E. R. Engdahl, *Geophys. J. Int.* **105**, 429 (1991).
26. A. M. Dziewonski, D. L. Anderson, *Phys. Earth Planet. Int.* **25**, 297 (1981).
27. S. Karato, *Geophys. Res. Lett.* **20**, 1623 (1993).
28. W. H. Press, S. A. Teukolsky, W. T. Vetterling, B. P. Flannery, *Numerical Recipes in FORTRAN* (Cambridge Univ. Press, New York, ed. 2, 1992).
29. The correlation of global maps of H_{TZ} obtained using SS precursors with tomographic TZ wavespeeds is weak (13), although consistent with the olivine Clapeyron slopes from (14).
30. Reference Earth Model Web site, http://mahi.ucsd.edu/Gabi/rem.html.
31. T. W. Becker, L. Boschi, *Geochem. Geophys. Geosyst.* **3**, paper no. 2001GC000168 (2002).
32. L. Stixrude, *J. Geophys. Res.* **102**, 14835 (1997).
33. T. Irifune, M. Isshiki, *Nature* **392**, 702 (1998).
34. C. Bina, *Nature* **392**, 650 (1998).
35. J. E. Vidale, H. M. Benz, *Nature* **356**, 678 (1992).
36. C. W. Wicks, M. A. Richards, *Science* **261**, 1424 (1993).
37. S. Lebedev, S. Chevrot, R. D. van der Hilst, in preparation.
38. G. Nolet, *J. Geophys. Res.* **95**, 8499 (1990).
39. We thank A. Zielhuis for running the resolution tests for the tomographic model of Australia. This work was supported by the David and Lucile Packard Foundation through a fellowship awarded to R.D.v.d.H.

Identity and Search in Social Networks

Duncan J. Watts,[1,2,3]* Peter Sheridan Dodds,[2] M. E. J. Newman[3]

Social networks have the surprising property of being "searchable": Ordinary people are capable of directing messages through their network of acquaintances to reach a specific but distant target person in only a few steps. We present a model that offers an explanation of social network searchability in terms of recognizable personal identities: sets of characteristics measured along a number of social dimensions. Our model defines a class of searchable networks and a method for searching them that may be applicable to many network search problems, including the location of data files in peer-to-peer networks, pages on the World Wide Web, and information in distributed databases.

In the late 1960s, Travers and Milgram (1) conducted an experiment in which randomly selected individuals in Boston, Massachusetts, and Omaha, Nebraska, were asked to direct letters to a target person in Boston,

each forwarding his or her letter to a single acquaintance whom they judged to be closer than themselves to the target. Subsequent recipients did the same. The average length of the resulting acquaintance chains for the let-

ters that eventually reached the target (roughly 20%) was about six. This reveals not only that short paths exist (*2*, *3*) between individuals in a large social network but that ordinary people can find these short paths (*4*). This is not a trivial statement, because people rarely have more than local knowledge about the network. People know who their friends are. They may also know who some of their friends' friends are. But no one knows the identities of the entire chain of individuals between themselves and an arbitrary target.

The property of being able to find a target quickly, which we call searchability, has been shown to exist in certain specific classes of networks that either possess a certain fraction of hubs [highly connected nodes which, once reached, can distribute messages to all parts of the network (*5–7*)] or are built upon an underlying geometric lattice that acts as a proxy for "social space" (*4*). Neither of these network types, however, is a satisfactory model of society.

Here, we present a model for a social network that is based upon plausible social structures and offers an explanation for the phenomenon of searchability. Our model follows naturally from six contentions about social networks.

1) Individuals in social networks are endowed not only with network ties, but identities (*8*): sets of characteristics attributed to them by themselves and others by virtue of their association with, and participation in, social groups (*9*, *10*). The term "group" refers to any collection of individuals with which some well-defined set of social characteristics is associated.

2) Individuals break down, or partition, the world hierarchically into a series of layers, where the top layer accounts for the entire world and each successively deeper layer represents a cognitive division into a greater number of increasingly specific groups. In principle, this process of distinction by division can be pursued all the way down to the level of individuals, at which point each person is uniquely associated with his or her own group. For purposes of identification, however, people do not typically do this, instead terminating the process at the level where the corresponding group size *g* becomes cognitively manageable. Academic departments, for example, are sometimes small enough to function as a single group but tend to split into specialized subgroups as they grow larger. A reasonable upper bound

on group size (*9*) is $g \cong 100$, a number that we incorporate into our model (Fig. 1A). We define the similarity x_{ij} between individuals i and j as the height of their lowest common ancestor level in the resulting hierarchy, setting $x_{ij} = 1$ if i and j belong to the same group. The hierarchy is fully characterized by depth l and constant branching ratio b. The hierarchy is a purely cognitive construct for measuring social distance, and not an actual network. The real network of social connections is constructed as follows.

3) Group membership, in addition to defining individual identity, is a primary basis for social interaction (*10*, *11*) and therefore acquaintanceship. As such, the probability of acquaintance between individuals i and j decreases with decreasing similarity of the groups to which they respectively belong. We model this by choosing an individual i at random and a link distance x with probability $p(x) = c \exp[-\alpha x]$, where α is a tunable parameter and c is a normalizing constant. We then choose a second node j uniformly among all nodes that are a distance x from i, repeating this process until we have constructed a network in which individuals have an average number of friends z. The parameter α is therefore a measure of homophily—the tendency of like to associate with like. When $e^{-\alpha} \ll 1$, all links will be as short as possible, and individuals will connect only to those most similar to themselves (i.e., members of their own bottom-level group), yielding a completely homophilous world of isolated cliques. By contrast, when $e^{-\alpha} = b$, any individual is equally likely to interact with any other, yielding a uniform random graph (*12*) in which the notion of individual similarity or dissimilarity has become irrelevant.

4) Individuals hierarchically partition the

social world in more than one way (for example, by geography and by occupation). We assume that these categories are independent, in the sense that proximity in one does not imply proximity in another. For example, two people may live in the same town but not share the same profession. In our model, we represent each such social dimension by an independently partitioned hierarchy. A node's identity is then defined as an H-dimensional coordinate vector $\vec{v}_i$, where v_i^h is the position of node i in the hth hierarchy, or dimension. Each node i is randomly assigned a coordinate in each of H dimensions and is then allocated neighbors (friends) as described above, where now it randomly chooses a dimension h (e.g., occupation) to use for each tie. When $H = 1$ and $e^{-\alpha} \ll 1$, the density of network ties must obey the constraint $z < g$.

5) On the basis of their perceived similarity with other nodes, individuals construct a measure of "social distance" y_{ij}, which we define as the minimum ultrametric distance over all dimensions between two nodes i and j; i.e., $y_{ij} = \min_h x_{ij}^h$. This minimum metric captures the intuitive notion that closeness in only a single dimension is sufficient to connote affiliation (for example, geographically and ethnically distant researchers who collaborate on the same project). A consequence of this minimal metric, depicted in Fig. 1B, is that social distance violates the triangle inequality—hence it is not a true metric distance—because individuals i and j can be close in dimension h_1, and individuals j and k can be close in dimension h_2, yet i and k can be far apart in both dimensions.

6) Individuals forward a message to a single neighbor given only local information about the network. Here, we suppose that
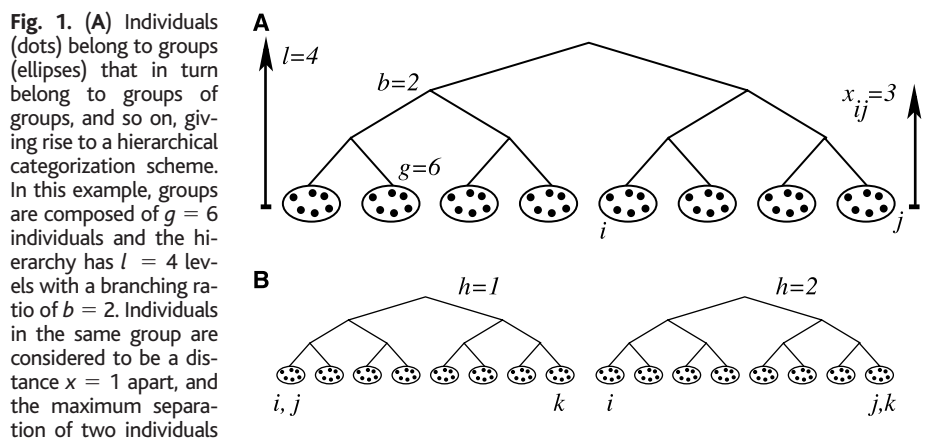

Fig. 1. (**A**) Individuals (dots) belong to groups (ellipses) that in turn belong to groups of groups, and so on, giving rise to a hierarchical categorization scheme. In this example, groups are composed of $g = 6$ individuals and the hierarchy has $l = 4$ levels with a branching ratio of $b = 2$. Individuals in the same group are considered to be a distance $x = 1$ apart, and the maximum separation of two individuals is $x = l$. The individuals i and j belong to a category two levels above that of their respective groups, and the distance between them is $x_{ij} = 3$. Individuals each have z friends in the model and are more likely to be connected with each other the closer their groups are. (**B**) The complete model has many hierarchies indexed by $h = 1 \ldots H$, and the combined social distance y_{ij} between nodes i and j is taken to be the minimum ultrametric distance over all hierarchies $y_{ij} = \min_h x_{ij}^h$. The simple example shown here for $H = 2$ demonstrates that social distance can violate the triangle inequality: $y_{ij} = 1$ because i and j belong to the same group under the first hierarchy and similarly $y_{jk} = 1$ but i and k remain distant in both hierarchies, giving $y_{ik} = 4 > y_{ij} + y_{jk} = 2$.

[1]Department of Sociology, Columbia University, New York, NY 10027, USA. [2]Columbia Earth Institute, Columbia University, New York, NY 10027, USA. [3]Santa Fe Institute, 1399 Hyde Park Road, Santa Fe, NM 87501, USA.

*To whom correspondence should be addressed. E-mail: djw24@columbia.edu

each node i knows only its own coordinate vector $\vec{v}_i$, the coordinate vectors $\vec{v}_j$ of its immediate network neighbors, and the coordinate vector of a given target individual $\vec{v}_t$, but is otherwise ignorant of the identities or network ties of nodes beyond its immediate circle of acquaintances.

Individuals therefore have two kinds of partial information: social distance, which can be measured globally but which is not a true distance (and hence can yield misleading estimates); and network paths, which generate true distances but which are known only locally. Although neither kind of information alone is sufficient to perform efficient search-

es, here we show that a simple algorithm that combines knowledge of network ties and social identity can succeed in directing messages efficiently. The algorithm we implement is the same greedy algorithm Milgram suggested: Each member i of a message chain forwards the message to its neighbor j who is closest to the target t in terms of social distance; that is, y_{jt} is minimized over all j in i's network neighborhood.

Our principal objective is to determine the conditions under which the average length $\langle L \rangle$ of a message chain connecting a randomly selected sender s to a random target t is small. Although "small" has recently been

taken to mean that $\langle L \rangle$ grows slowly with the population size N (13, 14), Travers and Milgram found only that chain lengths were short. Furthermore, these message chains had to be short in an absolute sense because at each step, they were observed to terminate with probability $p \cong 0.25$ (1, 15). We therefore adopt a more realistic, functional notion of efficient search, defining for a given message failure probability p, a searchable network as any network for which q, the probability of an arbitrary message chain reaching its target, is at least a fixed value r. In terms of chain length, we formally require $q = \langle (1 - p)^L \rangle \geq r$, and from this we can obtain an estimate of the maximum required $\langle L \rangle$ using the approximated inequality $\langle L \rangle \leq \ln r / \ln(1 - p)$. For the purposes of this study, we set $r = 0.05$ and $p = 0.25$, yielding the stringent requirement that $\langle L \rangle \leq 10.4$ independent of the population size N. Figure 2A presents a typical phase diagram in H and α, outlining the searchable network region for several choices of N, $g = 100$, and $z = g - 1 = 99$.

Our main result is that searchable networks occupy a broad region of parameter space (α, H) which, as we argue below, corresponds to choices of the model parameters that are the most sociologically plausible. Hence our model suggests that searchability is a generic property of real-world social networks. We support this claim with some further observations and demonstrate that our model can account for Milgram's experimental findings.

First, we observe that almost all searchable networks display $\alpha > 0$ and $H > 1$, consistent with the notion that individuals are essentially homophilous (that is, they associate preferentially with like individuals) but judge similarity along more than one social dimension. Neither the precise degree to which they are homophilous, nor the exact number of dimensions they choose to use, appears to be important—almost any reasonable choice will do. The best performance, over the largest interval of α, is achieved for $H = 2$ or 3—an interesting result in light of empirical evidence (16) that individuals across different cultures in small-world experiments typically use two or three dimensions when forwarding a message.

Second, as Fig. 2B shows, although increasing the number of independent dimensions from $H = 1$ yields a dramatic reduction in delivery time for values of $\alpha > 0$, this improvement is gradually lost as H is increased further. Hence the window of searchable networks in Fig. 2A exhibits an upper boundary in H. Because ties associated with any one dimension are allocated independently with respect to ties in any other dimension, and because for fixed average degree z, larger H necessarily implies fewer ties per dimen-

Fig. 2. (A) Regions in H-α space where searchable networks exist for varying numbers of individual nodes N (probability of message failure $p = 0.25$, branching ratio $b = 2$, group size $g = 100$, average degree $z = g - 1 = 99$, 10^5 chains sampled per network). The searchability criterion is that the probability of message completion q must be at least $r = 0.05$. The lines correspond to boundaries of the searchable network region for $N = 102,400$ (solid), $N = 204,800$ (dot-dash), and $N = 409,600$ (dash). The region of searchable networks shrinks with N, vanishing at a finite value of N that depends on the model parameters. Note that $z < g$ is required to explore H-α space because for $H = 1$ and α sufficiently large, an individual's neighbors must all be contained within their sole local group. **(B)** Probability of message completion $q(H)$ when $\alpha = 0$ (squares) and $\alpha = 2$ (circles) for the $N = 102,400$ data set used in (A). The horizontal line shows the position of the threshold $r = 0.05$. Open symbols indicate that the network is searchable ($q \geq r$) and closed symbols mean otherwise. For $\alpha = 0$, searchability degrades with each additional hierarchy. For the homophilous case of $\alpha = 2$ with a single hierarchy, less than 1% of all searches find their target ($q \cong 0.004$). Adding just one other hierarchy increases the success rate to $q \cong 0.144$, and q slowly decreases with H thereafter.
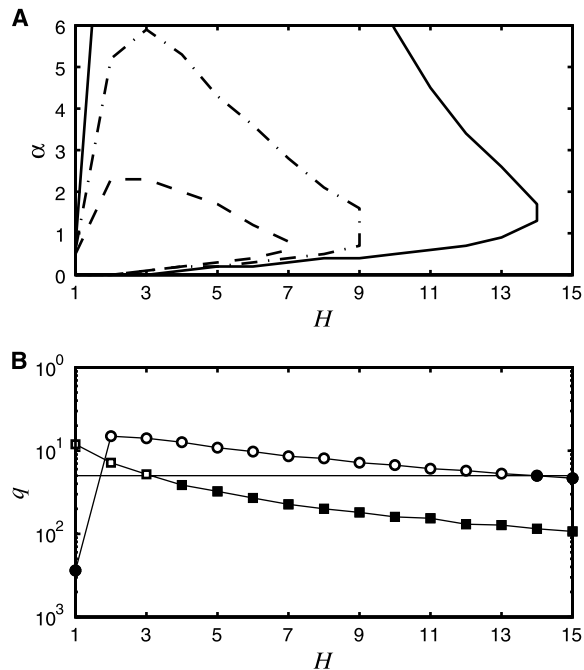

Fig. 3. Comparison between $n(L)$, the number of completed chains of length L, taken from the original small-world experiment (1) (bar graph) and from an example of our model with $N = 10^8$ individuals (filled circles with the line being a guide for the eye). The experimental data shown are for the 42 completed chains that originated in Nebraska. (We have excluded the 24 completed chains that originated in Boston as this would correspond to $N \cong 10^6$.) The model parameters are $H = 2$, $\alpha = 1$, $b = 10$, $g = 100$, and $z = 300$; message attrition rate is set at 25%; $n(L)$ for the model is compiled from 10^6 random chains and is normalized to match the 42 completed chains that started in Nebraska. The average chain length of Milgram's experiment is ~ 6.5, whereas the model yields $\langle L \rangle \cong 6.7$. The distributions compare well: A two-sided Kolmogorov-Smirnov test yields a P-value of $P \cong 0.57$, whereas for a χ^2 test, $\chi^2 \cong 5.46$ and $P \cong 0.49$ (seven bins). (A large value of P supports the hypothesis that the distributions are similar.) Even without attrition, the model's average search time is $\langle L \rangle \cong 8.5$ and the median chain length is 8. The model does not entirely match the experimental data because the former requires approximately 360 initial chains to achieve 42 completions as compared with 196.
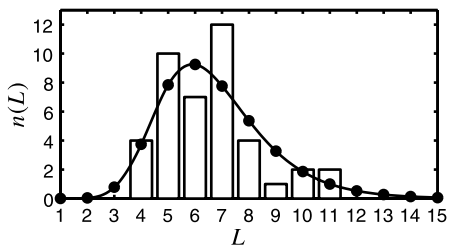
sion, the network ties become less correlated as H increases. In the limit of large H, the network becomes essentially a random graph (regardless of α) and the search algorithm becomes a random walk. An effective decentralized search therefore requires a balance (albeit a highly forgiving one) of categorical flexibility and constraint.

Finally, by introducing parameter choices that are consistent with Milgram's experiment ($N = 10^8$, $p = 0.25$) (1), as well as with subsequent empirical findings ($z = 300$, $H = 2$) (17, 16), we can compare the distribution of chain lengths in our model with that of Travers and Milgram (1) for plausible values of α and b. As Fig. 3 shows, we obtain $\langle L \rangle \cong 6.7$ for $\alpha = 1$ and $b = 10$, indicating that our model captures the essence of the real small-world problem. This agreement is robust with respect to variations in the branching ratio, showing little change over the range $5 < b < 50$.

Although sociological in origin, our model is relevant to a broad class of decentralized search problems, such as peer-to-peer networking, in which centralized servers are excluded either by design or by necessity, and where broadcast-type searches (i.e., forwarding messages to all neighbors rather than just one) are ruled out because of congestion constraints (6). In essence, our model applies to any data structure in which data elements exhibit quantifiable characteristics analogous to our notion of identity, and similarity between two elements— whether people, music files, Web pages, or research reports—can be judged along more than one dimension. One of the principal difficulties with designing robust databases (18) is the absence of a unique classification scheme that all users of the database can apply consistently to place and locate files. Two musical songs, for example, can be similar because they belong to the same genre or because they were created in the same year. Our model transforms this difficulty into an asset, allowing all such classification schemes to exist simultaneously, and connecting data elements preferentially to similar elements in multiple dimensions. Efficient decentralized searches can then be conducted by means of simple, greedy algorithms providing only that the characteristics of the target element and the current element's immediate neighbors are known.

References and Notes
1. J. Travers, S. Milgram, *Sociometry* **32**, 425 (1969).
2. D. J. Watts, S. J. Strogatz, *Nature* **393**, 440 (1998).
3. S. H. Strogatz, *Nature* **410**, 268 (2001).
4. J. Kleinberg, *Nature* **406**, 845 (2000).
5. A.-L. Barabási, R. Albert, *Science* **286**, 509 (1999).
6. L. Adamic, R. Lukose, A. Puniyani, B. Huberman, *Phys. Rev. E* **64**, 046135 (2001).
7. B. J. Kim, C. N. Yoon, S. K. Han, H. Jeong, *Phys. Rev. E* **65**, 027103 (2002).
8. H. C. White, *Identity and Control* (Princeton Univ. Press, Princeton, NJ, 1992).
9. G. Simmel, *Am. J. Sociol.* **8**, 1 (1902).
10. F. S. Nadel, *Theory of Social Structure* (Free Press, Glencoe, IL, 1957).
11. R. Breiger, *Social Forces* **53**, 181 (1974).
12. B. Bollobás, *Random Graphs* (Academic Press, New York, 1985).
13. M. Newman, D. Watts, *Phys. Rev. E* **60**, 7332 (1999).
14. J. Kleinberg, *Proc. 32nd ACM Symposium on Theory of Computing* (Association for Computing Machinery, New York, 2000).
15. H. C. White, *Social Forces* **49**, 259 (1970).
16. H. Bernard, P. Killworth, M. Evans, C. McCarty, G. Shelly, *Ethnology* **27**, 155 (1988).
17. P. Killworth, H. Bernard, *Soc. Networks* **1**, 159 (1978).
18. B. Manneville, *The Biology of Business: Decoding the Natural Laws of the Enterprise* (Jossey-Bass, San Francisco, 1999), chap. 5.
19. We thank J. Kleinberg for beneficial discussions. This work was funded in part by the National Science Foundation (grants SES-00-94162 and DMS-0109086), the Intel Corporation, and the Columbia University Office of Strategic Initiatives.

Ascent of Dinosaurs Linked to an Iridium Anomaly at the Triassic-Jurassic Boundary

P. E. Olsen,[1] D. V. Kent,[1,2] H.-D. Sues,[3] C. Koeberl,[4] H. Huber,[4] A. Montanari,[5] E. C. Rainforth,[1] S. J. Fowell,[6] M. J. Szajna,[7] B. W. Hartline[7]

Analysis of tetrapod footprints and skeletal material from more than 70 localities in eastern North America shows that large theropod dinosaurs appeared less than 10,000 years after the Triassic-Jurassic boundary and less than 30,000 years after the last Triassic taxa, synchronous with a terrestrial mass extinction. This extraordinary turnover is associated with an iridium anomaly (up to 285 parts per trillion, with an average maximum of 141 parts per trillion) and a fern spore spike, suggesting that a bolide impact was the cause. Eastern North American dinosaurian diversity reached a stable maximum less than 100,000 years after the boundary, marking the establishment of dinosaur-dominated communities that prevailed for the next 135 million years.

One of the most striking events in the Mesozoic was the rise to dominance of dinosaurs in terrestrial ecosystems. The cause and timing of their early Mesozoic ascent have been debated (1–4), with difficulties in global correlation and low sampling density limiting the utility of global compilations and obscuring relations to possible forcing mechanisms. However, terrestrial vertebrate assemblages in eastern North America are temporally better constrained than elsewhere and provide high-resolution biological and geochemical data bearing on this issue. This region was within the tropics during the Triassic and contained rift valleys, which were formed during the incipient fragmentation of Pangea. These basins contain kilometer-thick sections of continental strata, termed the Newark Supergroup, which have recorded the rise of dinosaurs across 15° of paleolatitude (5). Milankovitch-type climate cycles permeate the lacustrine strata of these basins, and in conjunction with paleomagnetic reversal stratigraphy, all of the

fossils can be placed within a high-resolution astronomically tuned time scale (6, 7) (Fig. 1).

Here, we focus on material from 80 localities in four Newark Supergroup basins, consisting of reptile footprints (8, 9), skeletal remains (2, 10), and palynological material (11) keyed into the astronomically tuned time scale (Figs. 1 and 2). The footprints are abundant, well-preserved, and diverse, and they offer a temporal sampling of terrestrial vertebrate communities that is better than the sampling from skeletal material around the Triassic-Jurassic boundary (4, 8). On the basis of comparisons between the reconstructed osteology of footprints and known skeletal remains, the ichnogenus level generally corresponds to an osteological family or higher taxonomic level (Table 1). However, footprints sample the terrestrial communities directly, and major changes in footprint assemblage composition probably represent important ecological changes (12). Even with uncertainty in the nature of the trackmakers, well-preserved footprints offer a useful independent proxy of faunal change (13), and the observed stratigraphic changes in the ichnological assemblages are consistent with the changes seen in osteological remains (Fig. 1).

On the basis of compiled ranges tied to the time scale (Fig. 1), Newark Supergroup dinosaurian ichnotaxa show a slow increase in relative abundance and a stepped increase in maximum size below the Triassic-Jurassic boundary (9). The ornithischian dinosaurian ichnogenus *Atreipus* (14) is the most common dinosaurian

[1]Lamont-Doherty Earth Observatory of Columbia University, Palisades, NY 10964, USA. [2]Department of Geological Sciences, Rutgers University, Piscataway, NJ 08854−8066, USA. [3]Department of Palaeobiology, Royal Ontario Museum, 100 Queen's Park, Toronto, ON M5S 2C6, Canada. [4]Institute of Geochemistry, University of Vienna, Althanstrasse 14, A-1090 Vienna, Austria. [5]Osservatorio Geologio do Coldigiocom, 1-62020 Frontale di Aprio, Italy. [6]Department of Geology and Geophysics, University of Alaska Fairbanks, Fairbanks, AK 99775−5780, USA. [7]Reading Public Museum, 500 Museum Road, Reading, PA 19611, USA.